Simulation of Semiconductor Processes and Devices 2016
Edited by E. Bär, J. Lorenz, and P. Pichler

Noise Simulation of Bipolar Organic Semiconductor Devices Based on the Master Equation

Weifeng Zhou, Christoph Zimmermann, Christoph Jungemann
Chair of Electromagnetic Theory
RWTH Aachen University
Aachen 52056, Germany
Email: wz@ithe.rwth-aachen.de

***Abstract*—Noise analysis in bipolar organic semiconductor devices is performed via the Langevin approach for a three-dimensional master equation under the sinusoidal steady-state condition. A single-layer diode with a cubic lattice is investigated. Hopping, generation and recombination of charge carriers are all treated as Poisson processes. Calculations of the power spectral density of the terminal current show the noise dependence on frequency, bias, position, device thickness, recombination lifetime and energetic disorder.**

I. Introduction

The reliability and durability of organic semiconductor devices are critical issues impeding their industrial applications. It has been shown that the noise spectrum is a sensitive diagnostic tool to detect early failures [1], [2], e.g. due to defects, and offers indications for effects like degradation [3], [4].

Noise in electronic devices originates from collective fluctuations of charge carrier velocity and population [5]. Most studies on noise analysis concerned only semi-analytical models [6], [7] and little attention was paid to the comprehensive noise analysis within physics-based models. Noise evaluation of a 2D pn diode was implemented in [5] via the Langevin approach within the drift-diffusion (DD) model. In organic devices, advancement has been made in [8] based on the unipolar master equation (ME), which shows closer relation to the underlying physics of organic semiconductors than the DD model does. In this paper, based on the bipolar ME model introduced in [9] with a crucial parameter of recombination lifetime, we present the first simulation of current noise in bipolar organic semiconductor diodes. For simplicity, only the trap-free condition is considered.

II. Approach

The time-dependent bipolar MEs for electron and hole occupancies p_i^e and p_i^h, respectively, at site i were formulated as [9]

$$\frac{dp_i^e}{dt} = \sum_{j\neq i} \left[p_j^e w_{ji}^e (1-p_i^e) - p_i^e w_{ij}^e (1-p_j^e)\right] - R_i + G_i, \tag{1a}$$

$$\frac{dp_i^h}{dt} = \sum_{j\neq i} \left[p_j^h w_{ji}^h (1-p_i^h) - p_i^h w_{ij}^h (1-p_j^h)\right] - R_i + G_i, \tag{1b}$$

with R_i and G_i indicating the direct recombination and generation rates, respectively. These rates are controlled by a recombination lifetime τ and a generation lifetime τ/c_i, in which c_i ensures the principle of detailed balance [9].

The Miller-Abrahams (M-A) hopping mechanism [10] is used. For electrons, the transition rates from site i to j read

$$w_{ij}^e = \begin{cases} \nu_0^e \exp\left[-2\alpha r_{ij} - \dfrac{E_j^e - E_i^e}{k_B T}\right], & E_j^e \geq E_i^e \\ \nu_0^e \exp\left[-2\alpha r_{ij}\right], & E_j^e < E_i^e \end{cases}, \tag{2}$$

with a similar formulation for holes. ν_0^e and ν_0^h are their respective hopping prefactors, α is a measure for the strength of carrier localization, and r_{ij} is the distance between sites i and j. The site energy E is a superposition of an intrinsic energy, the image potential and the quasi-static potential obtained by the 1D Poisson equation. The intrinsic energy is randomly chosen from a Gaussian probability density function

$$g(\epsilon) = \frac{1}{\sqrt{2\pi}\sigma} \exp\left[-\frac{(\epsilon-\Delta)^2}{2\sigma^2}\right], \tag{3}$$

with a standard deviation σ indicating the energetic disorder and a mean energy Δ known as the lowest unoccupied molecular orbital (LUMO) energy for electrons and the highest occupied molecular orbital (HOMO) energy for holes. In our simulations, a dimensionless characteristic disorder parameter $\hat{\sigma}=\sigma/(k_B T)$ is used and equal differences between local HOMO and LUMO energies on each site are assumed.

Around the stationary solution from [9], the transient bipolar MEs and Poisson equation are linearized by a small-signal approach and solved for a vector of occupancy and potential phasors, $\underline{x}$, with Dirichlet boundary conditions. The small-signal terminal current can be obtained by linearization of the Ramo-Shockley-type current in [9], $\underline{I}=\underline{C}^T\underline{x}$. Based on the Green's functions $\underline{G}$, the transfer functions for the terminal current are expressed as $\underline{T}_I=\underline{G}^T\underline{C}$, by which the small-signal admittance $\underline{Y}$ is given [8].In the trap-free case, noise sources only appear in MEs. Regarding that the positions of initial and target sites for hopping of carriers differ in real space and generation and recombination (GR) occur locally, the total power spectral density (PSD) of the terminal current is

$$\begin{aligned} W_{I,I} =& 2\sum_t \sum_{i,j} p_i^t w_{ij}^t (1-p_j^t) \left|\underline{T}_{I,i}^t - \underline{T}_{I,j}^t - q_t \frac{x_j - x_i}{L_x}\right|^2 \\ &+ 2\sum_i (G_i + R_i) \left|\underline{T}_{I,i}^e + \underline{T}_{I,i}^h\right|^2, \end{aligned} \tag{4}$$

978-1-5090-0818-6/16/$31.00 ©2016 European Union

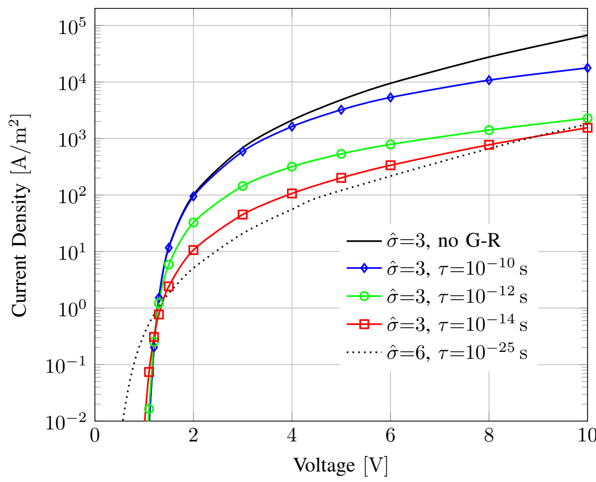

Fig. 1. IV characteristics of a symmetric bipolar diode for $\hat{\sigma}$=3 (solid) with various lifetimes and $\hat{\sigma}$=6 (dotted) with τ=10^{-25} s in the SCLC regime. Parameters follow those from [9]: hopping prefactors ν_0^e=ν_0^h=2.2×10^{17} s^{-1} for $\hat{\sigma}$=3 and ν_0^e=ν_0^h=2.2×10^{20} s^{-1} for $\hat{\sigma}$=6, temperature T=298 K, normalized disorder $\hat{\sigma}$=3, device thickness L=100 nm, lattice constant a_0=1 nm, built-in voltage V_{bi}=2 V, measure for localization α=10^8 cm^{-1}. All parameters not explicitly given in following figures take the values here.

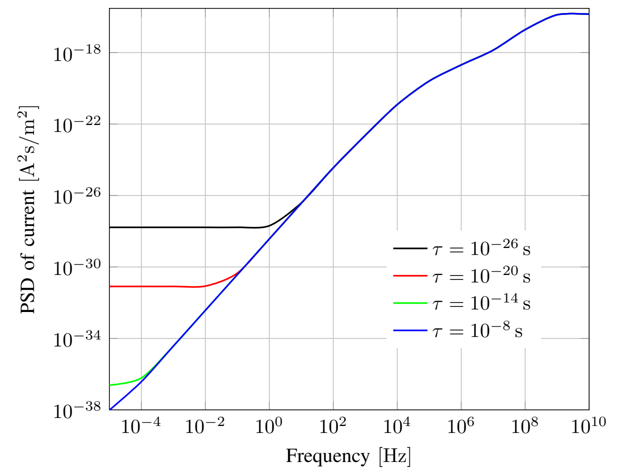

Fig. 2. Frequency-dependent thermal noise of the terminal current under equilibrium for $\hat{\sigma}$=3 with ascending lifetimes from top to bottom.

in which the fluctuations due to hopping of electrons (t=e) and holes (t=h) are explicitly included. The first summand denotes the noise from hopping of electrons and holes (hopping noise), the second one from GR of electron-hole pairs (GR noise).

The Newton-Raphson method was used to solve the problem self-consistently with quadratic convergence, and a cross-section of 50×50 sites was applied to all the simulations below.

III. Results and Discussion

A. IV Characteristics

The IV curves of a symmetric (ν_0^e=ν_0^h) bipolar diode under the influence of GR of arbitrary strength are plotted in Fig. 1. With sufficiently short lifetimes, the current saturates at the lower limit, where the space-charge-limited-current (SCLC) regime is reached. On the other hand, with long lifetimes, the recombination-limited-current (RLC) regime sets in and the current gradually increases to the case without GR. The hopping frequencies $\nu_0^{e,h}$ for $\hat{\sigma}$=6 were chosen to keep the current in the SCLC regime close to that for $\hat{\sigma}$=3.

B. Thermal Noise

The Nyquist theorem ($W_{I,I}$=$4k_BT\Re\{\underline{Y}\}$) is exactly followed for any value of lifetime under equilibrium, which validates our simulation approach. In Fig. 2, the low-frequency thermal noise continues becoming more pronounced even with extremely short lifetimes due to an increase in the GR noise, and it saturates at both the RLC and SCLC regime. However, such significant change in low-frequency noise over lifetime only happens under equilibrium, i.e. under non-equilibrium the noise in the SCLC regime saturates at longer lifetimes.

C. Hopping and GR Noise

For the non-equilibrium case, as shown in Fig. 3(a), the total low-frequency noise in the RLC regime is much higher

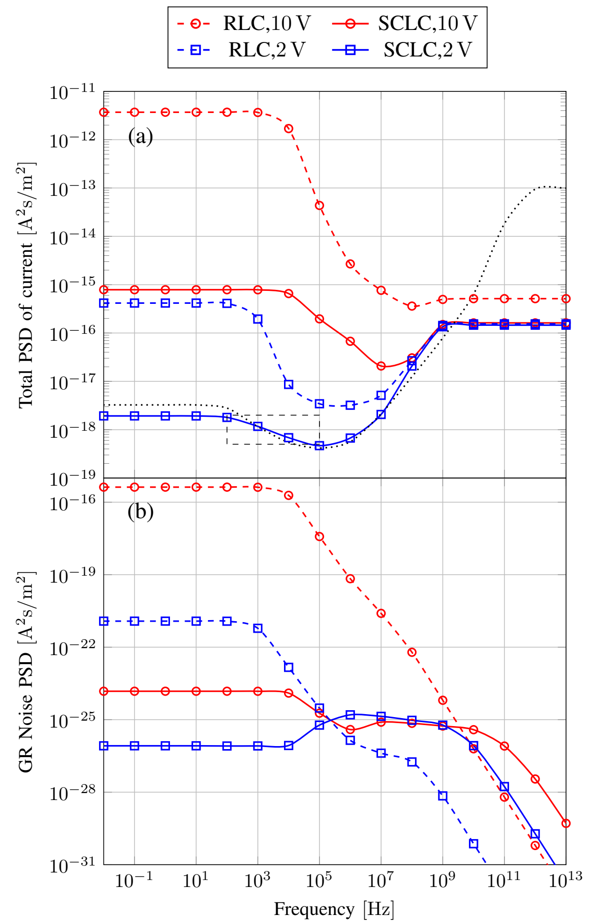

Fig. 3. Frequency-dependent (a) total noise and (b) GR noise PSD of the terminal current for $\hat{\sigma}$=3 at 2 V (square) and 10 V (circle) in the RLC (dashed) and SCLC (solid) regime (τ=10^{-6} s for RLC and 10^{-18} s for SCLC). Total noise PSD for $\hat{\sigma}$=6 (dotted) at 2 V in the SCLC regime is also plotted. The dashed rectangle indicates the range of $1/f^\beta$ noise for RLC at 2 V.

than that in the SCLC regime because of the much larger current. Based on the dispersive transport of injected charge carriers, noise shows a higher sensitivity to frequency in the RLC regime compared to the SCLC regime. The current

Simulation of Semiconductor Processes and Devices 2016
Edited by E. Bär, J. Lorenz, and P. Pichler

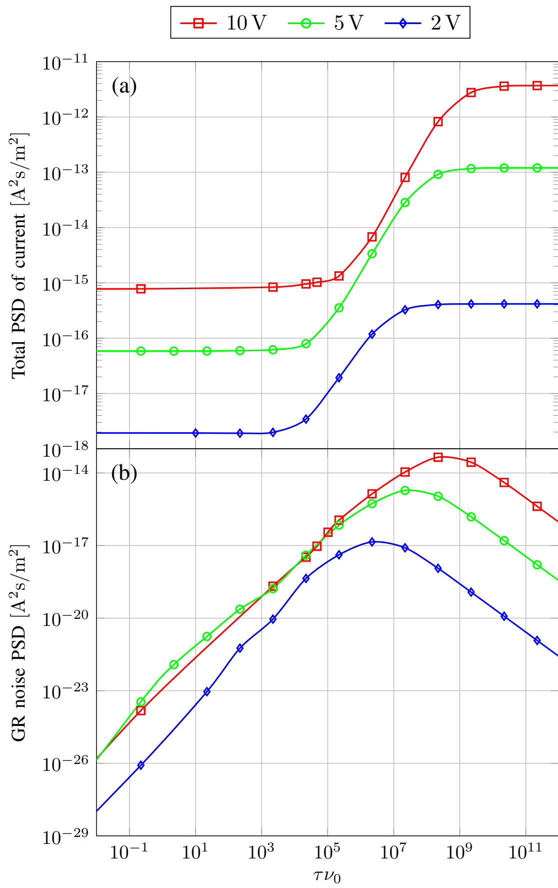

Fig. 4. Lifetime-dependent (a) total noise and (b) GR noise PSD of the terminal current for $\hat{\sigma}$=3 under various biases at 0 Hz.

noise for $\hat{\sigma}$=6 saturates at higher frequencies due to the higher hopping rates. Furthermore, the debatable $1/f^{\beta}$ noise [11], with a frequency coefficient β, only takes place in a narrow frequency range (indicated by a dashed rectangle as an example in Fig. 3(a)). It can be seen that longer lifetime or higher bias leads to larger β, and higher energetic disorder somewhat increases the slope of $1/f^{\beta}$ noise as well.

For comparison, the frequency-dependent GR noise is shown in Fig. 3(b). The GR noise is much lower than the hopping noise under forward bias, and its contribution vanishes by $1/f^2$ at high frequencies, which is a typical behavior of the Lorentzian-type noise spectrum [12]. Moreover, a combination of Lorentzians [12] can be found because of the different local relaxation rates of GR. Under equilibrium, the GR noise peak always appears in the low frequency regime. However, under non-equilibrium in the SCLC regime, the Lorentzian with a lower cut-off frequency turns into a negative contribution, which gives rise to a peak within the intermediate frequencies.

The total low-frequency current noise, which is depicted in Fig. 4(a), is more sensitive to lifetime within the transition region between the SCLC and RLC regime than the DC current (see Fig. 1). This indicates that the noise measurement is likely to be a more accurate way for determining the value of recombination lifetime. As plotted for comparison in Fig. 4(b), the GR noise reaches a peak within the transition region between the RLC and SCLC regime. In the SCLC regime

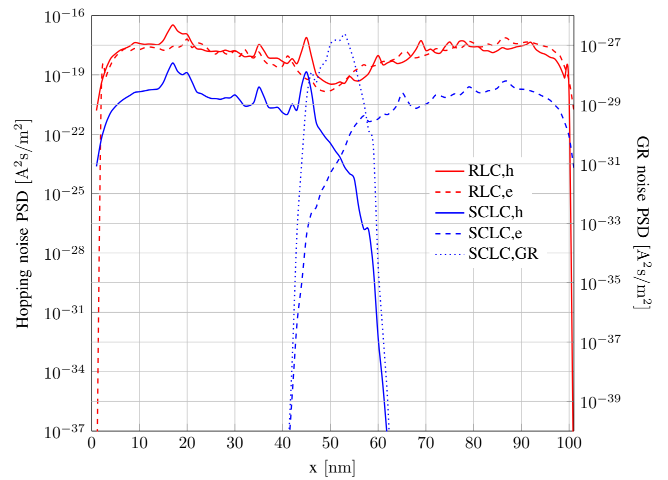

Fig. 5. Position-dependent hole (solid) and electron (dashed) hopping and GR noise (dotted) contributions in the RLC (τ=10^{-6} s) and SCLC (τ=10^{-18} s) regime for $\hat{\sigma}$=3 at 0 Hz and 2 V.

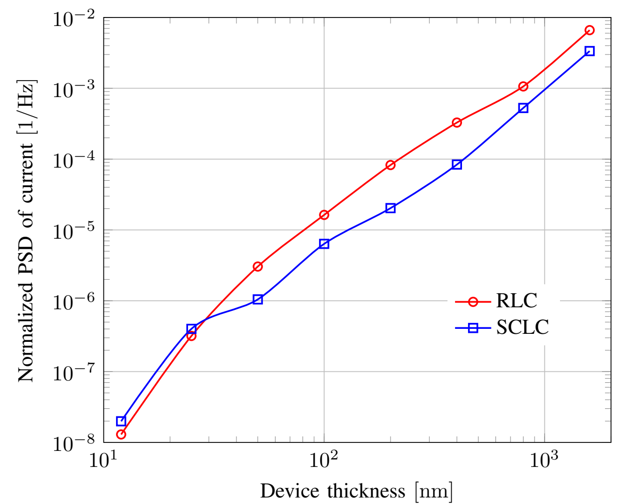

Fig. 6. Low-frequency normalized PSD of the terminal current as a function of the device thickness at 2 V in the RLC (circle, τ=10^{-6} s) and SCLC (square, τ=10^{-18} s) regime.

GR noise continuously decreases. This can be explained by the strong confinement of recombination in the center of the diode, where the fluctuations from GR take little effect.

The position-dependent low-frequency noise components from hopping and GR are plotted in Fig. 5. In the RLC regime, the hopping noise for each charge carrier type is almost symmetric, and the virtually constant transfer functions result in a valley in the diode center. In the SCLC regime, the hopping noise is mainly generated by the majorities, and the GR noise comes from the center of the symmetric device, at which GR processes mainly occur.

In order to investigate the influence of device thickness L on the noise behavior, the low-frequency normalized noise spectrum $\hat{W}$=$W_{I,I}/I^2$ is calculated. In Fig. 6, $\hat{W}$ shows a monotonic increase with L in both the RLC and SCLC regime. The reason is that, for a given bias, there are less injected charge carriers in a thicker diode, resulting in an increase

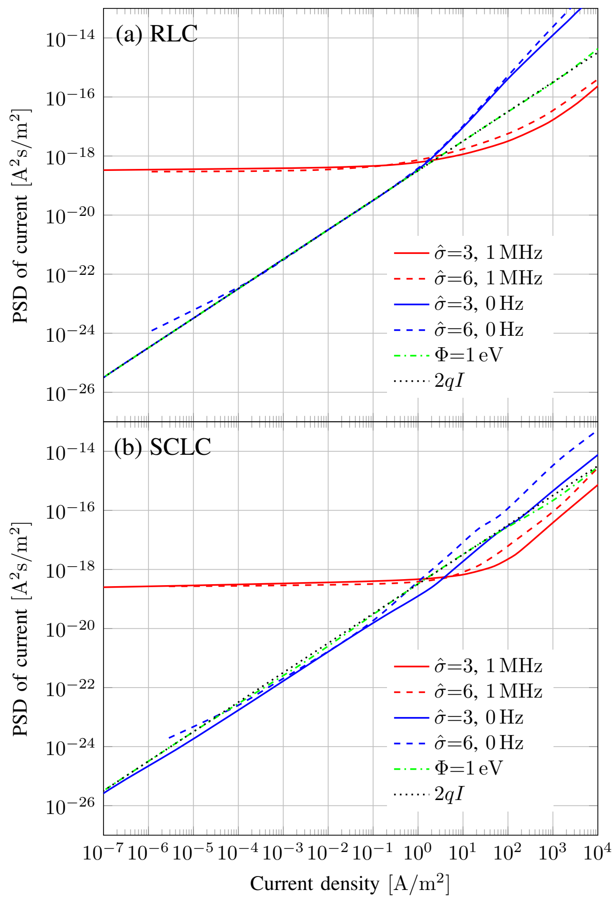

Fig. 7. PSD of the terminal current in the (a) RLC and (b) SCLC regime for $\hat{\sigma}$=3 (solid) and 6 (dashed) at both 0 Hz and 1 MHz as a function of the current, with comparison to shot noise (dotted). Results with high injection barrier of Φ=1 eV of both contacts for $\hat{\sigma}$=3 at 0 Hz are also depicted (dashdotted). For $\hat{\sigma}$=3, $\tau=10^{-6}$ s for RLC and 10^{-18} s for SCLC, and for $\hat{\sigma}$=6, $\tau=10^{-12}$ s for RLC and 10^{-25} s for SCLC.

in the effect of fluctuations. This also agrees with Hooge's empirical relation [11], in which $\hat{W}$ is inversely proportional to the charge carrier number. Moreover, such an effect has already been experimentally captured [13]. On the other hand, the normalized noise in the RLC regime is essentially higher than that in the SCLC regime for a given L. Only in very thin diodes, fluctuations due to minorities reaching the majority space charge regions become more pronounced in the SCLC regime.

D. Shot Noise

In the RLC regime, the low-frequency noise PSD follows shot noise ($2qI$), as shown in Fig. 7(a), for small terminal currents (e.g. with $V < V_{bi}$) and surpasses shot noise for sufficiently large currents due to the high injection of electrons and holes and their mutual charge compensation (see [9]). The thermal noise dominates under very low charge carrier injection. With higher injection barriers, deviation from shot noise prevails expectedly up to larger currents. In the SCLC regime (Fig. 7(b)), a small suppression of shot noise takes place, resulting from the Coulomb repulsion of space charges. Moreover, the low-frequency noise only exceeds shot noise for large currents, i.e. high injection, in which some electrons (holes) penetrate into the space charge region of holes (electrons). With high injection barriers, the low-frequency noise naturally approaches shot noise. On the other hand, the high-frequency current noise keeps constant for small current, followed by a sudden increase under high injection. Interestingly, the magnitude of energetic disorder has little effect on the current noise behavior.

IV. Conclusion

A ME-based current noise simulation has been performed via the Langevin approach under the sinusoidal steady-state condition. The approach is validated by the thermal noise being in agreement with the Nyquist theorem. Compared with the hopping noise, the GR noise is determined to be ignorable for the trap-free case under non-equilibrium. The higher sensitivity of low-frequency noise to the recombination lifetime demonstrates a more reliable way of measuring the value of lifetime than the IV characteristics. Deviation from shot noise occurs due to high charge carrier injections or formation of space charge regions.

References

[1] G. Ferrari, D. Natali, M. Sampietro, F. Wenzl, U. Scherf, C. Schmitt, R. Gntner, and G. Leising, "Current noise spectroscopy on mlppp based organic light emitting diodes," *Organic Electron.*, vol. 3, no. 1, pp. 33 – 42, 2002.

[2] P. R. F. Rocha, L. K. J. Vandamme, S. C. J. Meskers, H. L. Gomes, D. M. D. Leeuw, and P. van de Weijer, "Low-frequency noise as a diagnostic tool for oled reliability," in *Noise and Fluctuations (ICNF), 2013 22nd International Conference on*, June 2013, pp. 1–4.

[3] M. Sampietro, G. Ferrari, D. Natali, U. Scherf, K. O. Annan, F. P. Wenzl, and G. Leising, "Tracking of conduction phenomena and degradation in organic light emitting diodes by current noise measurements," *Appl. Phys. Lett.*, vol. 78, no. 21, pp. 3262–3264, 2001.

[4] L. Ke, H. Liu, M. Yang, Z. Jiao, and X. Sun, "Degradation analysis of Alq3-based OLED from noise fluctuations with different driving modes," *Chem. Phys. Lett.*, vol. 623, pp. 68 – 71, 2015.

[5] F. Bonani, G. Ghione, M. R. Pinto, and R. K. Smith, "An efficient approach to noise analysis through multidimensional physics-based models," *IEEE Trans. Electron Devices*, vol. 45, no. 1, pp. 261–269, Jan 1998.

[6] C. H. Chen and M. J. Deen, "Direct calculation of metaloxidesemiconductor field effect transistor high frequency noise parameters," *J. Vac. Sci. Technol. A*, vol. 16, no. 2, pp. 850–854, 1998.

[7] M. Sanden, O. Marinov, M. J. Deen, and M. Ostling, "A new model for the low-frequency noise and the noise level variation in polysilicon emitter bjts," *IEEE Trans. Electron Devices*, vol. 49, no. 3, pp. 514–520, Mar 2002.

[8] C. Jungemann, "Simulation of electronic noise in disordered organic semiconductor devices based on the master equation," *J. Comp. Elec.*, vol. 14, no. 1, pp. 37–42, 2015.

[9] W. Zhou, C. Zimmermann, and C. Jungemann, "Simulation of bipolar organic semiconductor devices based on the master equation including generation and recombination," in *2015 International Conference on Simulation of Semiconductor Processes and Devices (SISPAD)*, Sept 2015, pp. 136–139.

[10] A. Miller and E. Abrahams, "Impurity conduction at low concentrations," *Phys. Rev.*, vol. 120, pp. 745–755, Nov 1960.

[11] F. Hooge and L. Vandamme, "Lattice scattering causes 1/f noise," *Phys. Lett. A*, vol. 66, no. 4, pp. 315 – 316, 1978.

[12] T. Kuhn, L. Reggiani, and L. Varani, "A model current spectral density for hotcarrier noise in semiconductors," *J. Appl. Phys.*, vol. 69, no. 10, pp. 7097–7101, 1991.

[13] L. Ke, S. B. Dolmanan, L. Shen, C. Vijila, S. J. Chua, R.-Q. Png, P.-J. Chia, L.-L. Chua, and P. K.-H. Ho, "Low frequency noise analysis on organic thin film transistors," *J. Appl. Phys.*, vol. 104, no. 12, 2008.